Progress In Electromagnetics Research M, Vol. 31, 159–169, 2013

PROPOSING A WAVELET BASED MESHLESS METHOD FOR SIMULATION OF CONDUCTING MATERIALS

Arman Afsari and Masoud Movahhedi*

Department of Electrical Engineering, Shahid Bahonar University of Kerman, 22 Bahman Blvd., Kerman, Iran

Abstract—This work focuses on the development of multiscale meshless technique in area of scattered fields from paramagnetic scatterers. The radial point interpolation method (RPIM), as the most common meshless technique, is employed for above purpose. Due to high frequency analysis, some special considerations must be applied, particularly in subdomains near the incident face. So, to ensure the accuracy, a multiscale meshless technique in wavelet frames sounds necessary. Simulating the scatterers using above method, specifically an elliptic paramagnetic scatterer, shows some efficient aspects such as less computational time and more precision compared with some other numerical methods.

1. INTRODUCTION

In controversy of computational electromagnetics, two important factors, i.e., computational time and the accuracy, are important properties which a method must prove them to show its validity. The factors become more significant when method is supposed to be used at high frequencies in which some nonlinear phenomena may appear.

The radial point interpolation method (RPIM) as one of the most common meshless techniques possesses higher accuracy than some other weak form numerical methods as finite element method (FEM). This fact comes from the functional approximation spaces that in contradiction with FEM, are not necessarily of polynomials [1]. Extending the range of approximations from polynomial to exponential and logarithmic spaces helps us model problems with discontinuity and abrupt changes more accurate. Indeed, polynomials are not always able to follow the solution function with abrupt changes quite as good as exponential and logarithmic functions.

Received 23 April 2013, Accepted 9 June 2013, Scheduled 14 June 2013

* Corresponding author: Masoud Movahhedi (movahhedi@ieee.org).

However, as the main disadvantage, the computational time of RPIM is more than some well established methods, e.g., FEM [2–7]. In computational process of RPIM, a middle matrix inversion step (MMIS) with the same dimensions such as the final matrix inversion step (FMIS) (if the system of equations solved by direct method) constructs the shape functions [1]. Afterwards, the shape functions construct the FMIS and problem will be solved.

In this paper, using some previously published papers on the application of wavelets in electromagnetics [8–12], a new RPIM supplemented by the wavelet frames, is proposed by which RPIM is able to simulate electromagnetic problems in multi scales with less computational time consumption. This supplement affords by an ability of proposing shape functions, directly, without any need to MMIS.

Consequently, the computational time of RPIM supplemented by wavelet frames is improved. This improvement confirms the generality of modified RPIM and provides a way through which the method is applicable to wider range of electromagnetic problems. To see the improvements in practice, the method is imposed to simulate a paramagnetic scatterer.

Rest of the paper is organized as follows. In Section 2 the mathematical concepts of RPIM is reviewed. Some terms as basis and shape functions are explained. The MMIS and FMIS are shown in RPIM calculation process. Then, Section 3 illustrates the multi scale RPIM in wavelet frames. Indeed, this section tries to discover some relations between approximation functions in wavelet and meshless techniques. These relations are used to propose shape functions, directly. Finally, Section 4 imposes the modified RPIM to analyze an elliptic paramagnetic scatterer to see the improvements in practice.

2. THE RADIAL POINT INTERPOLATION METHOD (RPIM)

Let consider the general form of 2D scalar wave equation as

$$\frac{\partial}{\partial x}\left(a_x \frac{\partial u}{\partial x}\right) + \frac{\partial}{\partial y}\left(a_y \frac{\partial u}{\partial y}\right) - gu = -f, \quad (x, y) \in \Omega \tag{1}$$

where Ω is the problem domain, and a_x, a_y, g and f are known functions, supplemented by the following Dirichlet and mixed boundary conditions.

$$u = b_0, \quad \text{on curve } L_1 \tag{2}$$

$$\left(a_x \frac{\partial u}{\partial x}\hat{i} + a_y \frac{\partial u}{\partial y}\hat{j}\right).\hat{n} + \gamma u = q, \quad \text{on curve } L_2 \tag{3}$$

where $L = L_1 + L_2$ is the counter, enclosing Ω with outward normal vector $\hat{n}$. Again, γ, q and b_0 are known functions [1].

Using Ritz's sense, the functional (weak form) of above equation along with its boundary conditions is as

$$F(u) = \frac{1}{2}\int_{\Omega}\left[a_x\left(\frac{\partial u}{\partial x}\right)^2 + a_y\left(\frac{\partial u}{\partial y}\right)^2 + gu^2 - 2fu\right]d\Omega + \int_{L_2}\left(\frac{\gamma}{2}u^2 - qu\right)dL_2 \tag{4}$$

The RPIM proposes the following approximation as the solution of (4)

$$\tilde{u}(x,y) = \tilde{u} = \sum_{i=1}^{n} a_i B_i(x,y) \tag{5}$$

where a_i is the coefficient, $B_i(x,y)$ the *basis function* of exponential or logarithmic type, both at ith node, and n the number of scattered nodes in the problem domain Ω.

One of the most common basis functions in RPIM is the exponential one by shape parameter α, as [1]

$$B_i(x,y) = \exp\left(-\alpha\left[(x-x_i)^2 + (y-y_i)^2\right]\right) \tag{6}$$

The matrix representation of (5) is as

$$\tilde{u} = AB^T \tag{7}$$

where $A = [a_1\ a_2\ a_3\ \ldots\ a_n]$, $B = [B_1\ B_2\ B_3\ \ldots\ B_n]$ and T indicates transpose. Even though (5) is a solution, but it must be rewritten according to the value of solution function at scattered nodes [1]. So, the RPIM proposes the following approximation, equivalent to (5), as

$$\tilde{u} = \sum_{i=1}^{n} u_i S_i(x,y) \tag{8}$$

where u_i is the value of solution function and S_i the *shape function*, both at ith node. The matrix representation of above equation is

$$\tilde{u} = US^T \tag{9}$$

To find the shape functions, a $(n \times n)$ MMIS is constructed as below

$$S^T = B^T B_0^{-1} \tag{10}$$

where

$$\mathbf{B}_0 = \begin{pmatrix} B_1(x_1,y_1) & \ldots & B_n(x_1,y_1) \\ B_1(x_2,y_2) & \ldots & B_n(x_2,y_2) \\ \vdots & \ddots & \vdots \\ B_1(x_n,y_n) & \ldots & B_n(x_n,y_n) \end{pmatrix} \tag{11}$$

To find a general view of the shape functions, one of them, i.e., a shape function based on the exponential basis function (6), is illustrated in Figure 1. Clearly, there is no obligation to truncate the shape function. Because, its support domain as a circle that contains 13 nodes, is small enough and the value of shape function is very negligible (≈ 0.00001) outside the support domain. However and in an engineering point of view, any consideration that reduces the computational time may be imposed into the problem to make it more efficient. So, for holding the matrix sparseness in programming, the electromagnetic researchers may set the value of shape function to zero out of the support domain. As seen in Figure 1 as a typical shape function, it possesses some evident properties such as

- Kronecker delta property,
- Smoothness,
- Even symmetry.

which have been explained in [1].
Afterwards, the system of equations is assembled substituting (8) into (4) as

$$U_{n\times 1} = [K_{ij}]^{-1}_{n\times n}[b_{i1}]_{n\times 1} \tag{12}$$

in which

$$K_{ij} = \int_{\Omega} \left[a_x \frac{\partial S_i}{\partial x}\frac{\partial S_j}{\partial x} + a_y \frac{\partial S_i}{\partial y}\frac{\partial S_j}{\partial y} + g S_i S_j \right] d\Omega + \int_{L_2} \gamma S_i S_j dL_2 \tag{13}$$

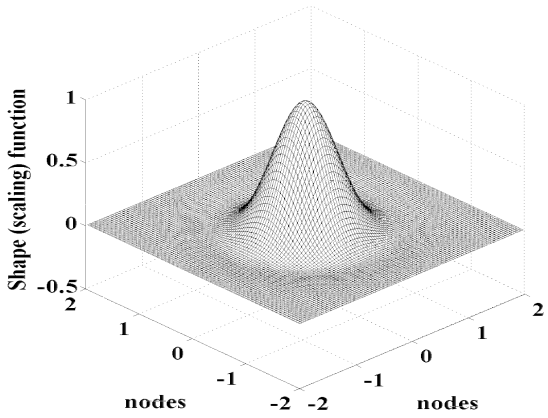

Figure 1. The shape function of RPIM with $x_i = y_i = 0$ as its center.

and

$$b_{i1} = \int_{\Omega} f S_i d\Omega + \int_{L_2} q S_i dL_2 \tag{14}$$

where the line integrals in (13) and (14) belong only to boundary nodes on L_2. In (12), the FMIS appears.

Both (10) and (12) take noticeable computational time in calculation process.

3. THE MODIFIED RADIAL POINT INTERPOLATION METHOD

In view of wavelet frames, a multiresolution equivalent for (8) is expressed as

$$\tilde{u}_{MRA}(x) = \sum_{J=0}^{J_{\max}} \sum_{i=1}^{n^J} \varphi\left(2^J x - i\right) u_i \tag{15}$$

where φ_i is the *scaling function* at ith node, n^J the number of scattered nodes at level J, $J_{\max}$ the maximum level of resolution, and $\sum_{J=0}^{J_{\max}} n^J = n$ [13]. Evidently, the role of scaling functions in wavelet frames and shape functions in meshless frames is the same.

In following theorem, the properties of scaling functions to construct a valid approximation and wavelet frame is expressed. This theorem discovers some connections between scaling and shape functions in each subdomain Ω_k.

Theorem 3.1 φ forms a valid wavelet frame if it satisfies the following conditions.

$$\text{support } (\varphi(x-k)) \subset \text{closure } (\Omega_k) \tag{16}$$

$$\varphi(x-k) \text{ be continuous on } \Omega_k \tag{17}$$

$$\int_{\Omega_k} \varphi(x-k)dx = 1 \tag{18}$$

$$\int_{\Omega_k} \varphi(x-k)\varphi(x-l)dx = \delta_{kl}^{Kronecker} \tag{19}$$

$$\varphi(2^j x - l) = \sum_{k \in Z} p_{k-2l} \varphi\left(2^{j+1} x - k\right) \tag{20}$$

Proof: See [13].

Putting the properties of both scaling and shape functions together, it sounds possible to work on an idea that proposes the shape functions, directly. In fact, eliminating the MMIS is the target of above idea for direct meshless method [14]. Let propose the following

class of functions as candidates for the aim which satisfy above scaling function and also shape function properties; this class is different than that of [15].

$$\varphi_i(x,y) = S_i(x,y) = \exp\left(-\alpha\left[(x-x_i)^2+(y-y_i)^2\right]\right) \times\left(-\beta\left[(x-x_i)^2+(y-y_i)^2\right]+1\right) \quad (21)$$

That contains two shape parameters α and β to control its shape. The proposed function (21), potentially, is able to satisfy all mentioned properties of scaling and shape functions. So, it is adequate to concentrate on finding the optimal values for α and β and matching (21) on Figure 1 [15]. For the sake of generality, $\alpha = 1.93$ and $\beta = 0.94$ are suggested as suitable values. As mentioned, the general criterion for above values are the three properties of shape functions in Section 2, i.e., Kronecker delta property, smoothness and even symmetry, beside those of scaling functions in theorem 3.1. Computational electromagnetic researchers may change above values for their specific problems. After all above theoretical efforts, the modified method must be imposed to a problem to show its validity in practice. As we expect, the computational cost should show a noticeable reduction. Next section realizes the application of modified RPIM.

4. ANALYSIS OF PARAMAGNETIC SCATTERERS

The problem under consideration, as a different class than [15], is depicted in Figure 2 where a source located somewhere in space illuminates an elliptic cylinder. In the absence of the scatterer, this source would produce a field filling all of space which is called the incident field. In the presence of the scatterer, it produces a different field, which is called the total field. The difference between total and

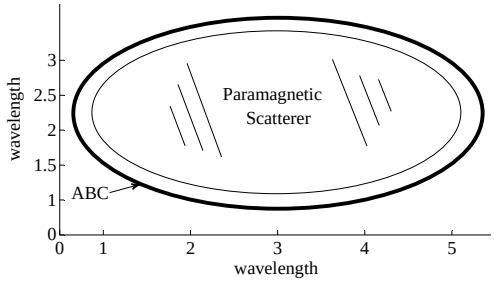

Figure 2. The paramagnetic scatterer and ABC.

incident fields is referred to as the scattered field. The problem is to determine the total or scattered fields which characterizes the scatterer. We apply both FEM and modified RPIM in conjunction with absorbing boundary conditions (ABCs) to the problem. In this analysis, the method of moments (MoM) is considered as the exact solution.

Clearly, any two dimensional wave can be decomposed to two electric and magnetic polarizations. Therefore, it suffices to consider these two fields, separately. According to Section 2, the following values are assigned to wave Equation (1) [16].

4.1. Electric Polarization

$$\begin{aligned} u &= E_z \\ a_x = a_y &= \frac{1}{\mu_r} \\ f &= -jk_0\eta_0 J_z \\ g &= -k_0^2\epsilon_r \end{aligned} \tag{22}$$

where k_0 is the wave number, η_0 the medium intrinsic impedance, and J_z the current density in z direction [16].

4.2. Magnetic Polarization

$$\begin{aligned} u &= H_z \\ a_x = a_y &= \frac{1}{\epsilon_r} \\ f &= \frac{\partial}{\partial x}\left(\frac{1}{\epsilon_r}J_y\right) - \frac{\partial}{\partial y}\left(\frac{1}{\epsilon_r}J_x\right) \\ g &= -k_0^2\mu_r \end{aligned} \tag{23}$$

Due to infinitely extension of the problem domain, it must be truncated; Consequently, a boundary condition must be introduced at artificial boundaries for a unique solution of the problem. One class of boundary conditions, i.e., absorbing boundary conditions (ABCs), lead to localized relations between the boundary fields; that is, they relate a field at a boundary node, only to those at neighboring nodes [16]. Consequently, a highly sparse coefficient matrix K is retained. Here, the following ABC (third kind boundary condition) for (3) is used to

truncate the domain.

$$\begin{aligned} \gamma &= a_x \left[jk_0 + \frac{k(s)}{2} \right] \\ q &= a_x \frac{\partial u^{inc}}{\partial n} + a_x \left[jk_0 + \frac{k(s)}{2} \right] u^{inc} \end{aligned} \tag{24}$$

where s is the arc length and $k(s)$ the curvature. The derivation of (24) can be found in [16].

The material of cylinder as a paramagnetic scatter is assumed to be Aluminium. This selection, practically, illustrates an important point of view when the main body material of many targets in radar theory are considered as Aluminium.

Choosing a uniform nodal distribution in each resolution level, and considering the left and right sides of the scatterer in which the curvature is more than other zones, as subdomains with higher resolution level, i.e., $J_{\max} = 3$, the problem is ready to be solved without MMIS. After some manipulations in weak form analysis proposed in previous sections, the system of equations is constructed to calculate the total field. Figures 3 and 4 show the electric and magnetic fields in the vicinity of cylinder illuminated by the following plane wave

$$u^{inc} = \exp\left(jk_0\left(x\cos\theta_{inc} + y\sin\theta_{inc}\right)\right) \tag{25}$$

with $\theta_{inc} = 0$. Figures 5 and 6 show the error analysis and computational time of FEM, conventional and modified RPIM. As seen, the modified RPIM reaches a given error order in less total number of nodes; therefore, less computational time and more accuracy than FEM is achieved which confirm the theoretical efforts.

It sounds necessary to mention how the resolution levels are set in Figure 5. Up to 290 nodes, the resolution level is set to zero and the

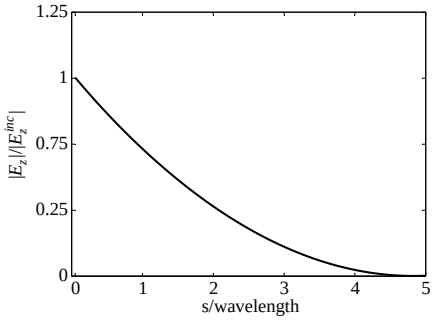

Figure 3. Electric field in vicinity of paramagnetic scatterer.

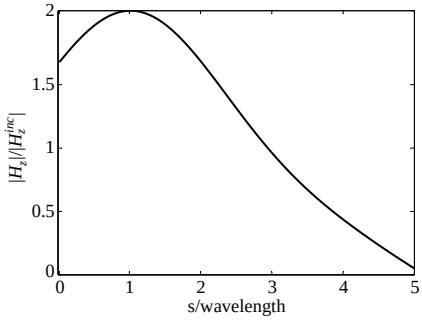

Figure 4. Magnetic field in vicinity of paramagnetic scatterer.

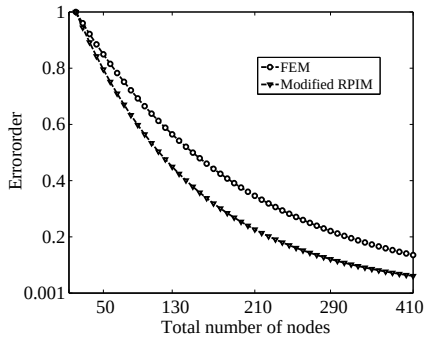

Figure 5. Error analysis of both FEM and modified RPIM.

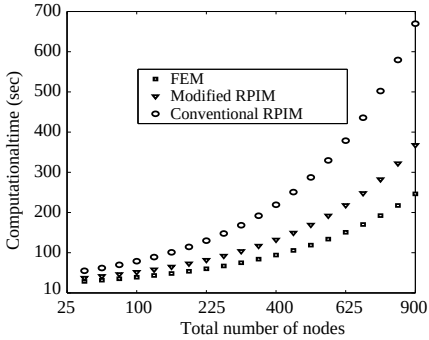

Figure 6. Computational time of FEM, conventional and modified RPIM.

uniform density of nodes is only increased. Then, the first resolution level ($J_{\max} = 1$) with 40 additional nodes is considered and the total number of nodes reaches 330. The problem is supplemented by second and third resolution levels, each one with 40 additional nodes. Hence, the total number of nodes is 370 and 410 for $J_{\max} = 2$ and $J_{\max} = 3$, respectively.

An interesting phenomenon in Figure 5 is that by increasing the resolution levels, the error plots of both methods tend toward their extremum points. Indeed, the minimum error degree of FEM lies higher than that of modified RPIM. Such minimum error degree confirms the effectiveness of using multiresolution methods instead of fixed level methods as FEM. So, the main disadvantage of meshless method, i.e., method computational time, is improved by proposing the shape functions, directly, using wavelet frames. In this problem,

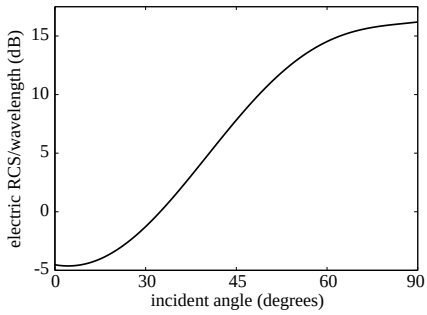

Figure 7. Backscattered RCS for electric field in vicinity of paramagnetic scatterer.

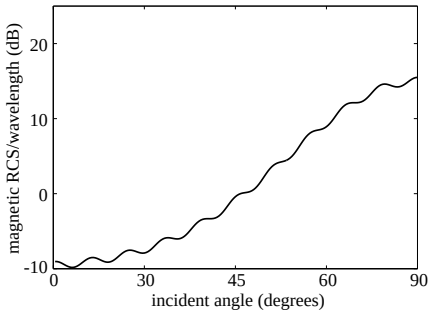

Figure 8. Backscattered RCS for magnetic field in vicinity of paramagnetic scatterer.

the conventional RPIM shows a very close error order to FEM and only the FEM error has been plotted, beside the modified RPIM.

Figures 7 and 8 show the backscattered radar cross section (RCS) for both polarizations versus angle of incident field. Due to good agreement between field values in modified RPIM and MoM, the RCSs of both polarizations are also in good agreement with those of MoM presented in [16].

5. CONCLUSION

This paper proposes a modified RPIM for which computational time has been improved. The basis of the work originates from a connection between scaling (wavelet frame) and shape (meshless frame) functions to provide some constraints by which the shape functions are proposed, directly, and the MMIS is canceled. The improved method was used to simulate a paramagnetic scatterer and showed good agreement with exact solution.

ACKNOWLEDGMENT

In accomplishing this paper, the authors gratefully acknowledge Prof. Holger Wendland, from Mathematical Institute, University of Oxford, for his instructions and steerage in area of using suitable constrains for shape functions.

REFERENCES

1. Liu, G. R. and Y. T. Gu, *An Introduction to Meshfree Methods and Their Programming*, Springer, New York, 2005.
2. Zhang, Y., K. R. Shao, D. X. Xie, and J. D. lavers, "Meshless method based on orthogonal basis for computational electromagnetics," *IEEE Trans. Magn.*, Vol. 41, No. 5, 1432–1435, May 2005.
3. Yang, S. Y., S. L. Ho, P. H. Ni, and G. Z. Ni, "A combined wavelet-FE method for transient electromagnetic-field computation," *IEEE Trans. Magn.*, Vol. 42, No. 4, 571–574, Apr. 2006.
4. Manzin, A. and O. Bottauscio, "Element-free Galerkin method for the analysis of electromagnetic-wave scattering," *IEEE Trans. Magn.*, Vol. 44, No. 6, 1366–1369, Jun. 2008.
5. Hubbert, S., "Closed form representations for a class of compactly supported radial basis functions," *Adv. Comput. Math.*, Vol. 36, 115–136, 2012.

6. Zhu, H., L. Tang, S. Song, Y. Tang, and D. Wang, "Symplectic wavelet collocation method for Hamiltonian wave equations," *J. Comput. Phys.*, Vol. 229, 2550–2572, 2010.
7. Davydova, O. and D. Oanh, "On the optimal shape parameter for Gaussian radial basis function finite difference approximation of the Poisson equation," *Comput. Math. Appl.*, Vol. 62, 2143–2161, 2011.
8. Zheng, G., B.-Z. Wang, H. Li, X.-F. Liu, and S. Ding, "Analysis of finite periodic dielectric gratings by the finite-difference frequency-domain method with the sub-entire-domain basis functions and wavelets," *Progress In Electromagnetic Research*, Vol. 99, 453–463, 2009.
9. Ala, G., E. Francomano, and F. Viola, "A wavelet operator on the interval in solving Maxwell's equations," *Progress In Electromagnetic Research Letters*, Vol. 27, 133–140, 2011.
10. Lashab, M., C. Zebiri, and F. Benabdelaziz, "Wavelet-based moment method and physical optics use on large reflector antennas," *Progress In Electromagnetic Research M*, Vol. 2, 189–200, 2008.
11. Iqbal, A. and V. Jeoti, "A novel wavelet-Galerkein method for modeling radio wave propagation in tropospheric ducts," *Progress In Electromagnetic Research B*, Vol. 36, 35–52, 2012.
12. Lashab, M., F. Benabdelaziz, and C.-E. Zebiri, "Analysis of electromagnetics scattering from reflector and cylindrical antennas using wavelet-based moment method," *Progress In Electromagnetic Research*, Vol. 76, 357–368, 2007.
13. Boggess, A. and F. J. Narcowich, *A First Course in Wavelets with Fourier Analysis*, Prentice Hall, Upper Saddle River, 2001.
14. Razmjoo, H., M. Movahhedi, and A. Hakimi, "Modification on a fast meshless method for electromagnetic field computations," *IET Sci. Meas. Technol.*, Vol. 5, No. 5, 175–182, Sep. 2011.
15. Afsari, A. and M. Movahhedi, "A modified wavelet-meshless method for lossy magnetic dielectrics at microwave frequencies," *IEEE Trans. Magn.*, Vol. 49, No. 3, 963–967, Mar. 2013.
16. Jin, J. M., *The Finite Element Method in Electromagnetics*, 2nd edition, John Wiley and Sons, Ltd., 2002.